

**JTECH-D-15-0149.s1**  
**Online Supplementary Materials**

**Performance evaluation of an integrated open-path eddy covariance system in a cold desert environment**

Wei Wang<sup>1,2</sup>, Jiaping Xu<sup>1</sup>, Yunqiu Gao<sup>1</sup>, Ivan Bogoev<sup>3</sup>, Jian Cui<sup>1</sup>, Lichen Deng<sup>1</sup>, Cheng Hu<sup>1</sup>, Cheng Liu<sup>1</sup>, Shoudong Liu<sup>1</sup>, Jing Shen<sup>1</sup>, Xiaomin Sun<sup>4</sup>, Wei Xiao<sup>1</sup>, Guofu Yuan<sup>4</sup>, Xuhui Lee<sup>1,5</sup>

1 Yale-NUIST Center on Atmospheric Environment, Nanjing University of Information Science and Technology, Nanjing 210044, China

2 Collaborative Innovation Center of Atmospheric Environment and Equipment Technology, Nanjing University of Information Science and Technology, Nanjing 210044, China

3 Research and Development, Campbell Scientific, Inc., Logan, UT 84321, USA

4 Key Laboratory of Ecosystem Network Observation and Modeling, Institute of Geographic Sciences and Natural Resources Research, Chinese Academy of Sciences, Beijing 100101, China

5 School of Forestry and Environmental Studies, Yale University, New Haven, CT 06511, USA

\* Author for correspondence

Dr. Xuhui Lee

Sara Shallenberger Brown Professor

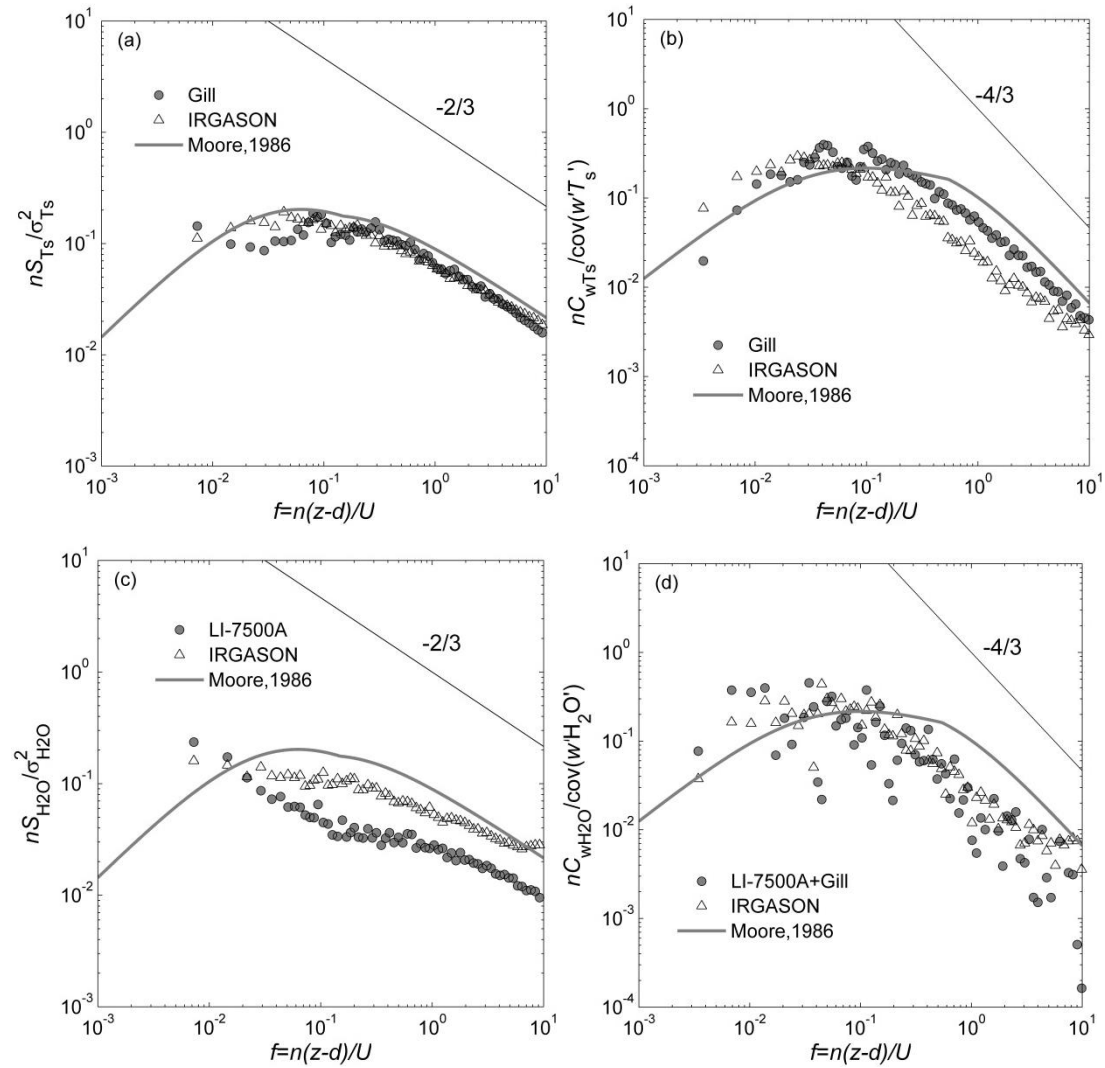
School of Forestry and Environmental Studies

Yale University

Kroon Hall, 195 Prospect Street, New Haven, CT 06511, USA

Phone: (203)432-6271; Fax: (203)432-5023; E-mail: [xuhui.lee@yale.edu](mailto:xuhui.lee@yale.edu)

Figure S1. Ensemble averaged normalized power spectra of sonic temperature (a)  $T_s$ , (c)  $H_2O$  and (e)  $CO_2$ , and (b)  $w-T_s$ , (d)  $w-H_2O$  and (f)  $w-CO_2$  cospectrum. Half-hour data from 10:00 to 13:00 local time over the winter experiment (from December 16, 2013 to January 3, 2014) were used. The spectra and cospectrum models of Moore (1986) are shown as the solid red line. The normalized surface layer frequency  $f=n(z-d)/U$  is used for the x-axis, where  $n$  (Hz) is the natural frequency,  $z$  (m) is the measurement height,  $d$  (m) is the zero-plane displacement, and  $U$  ( $m\ s^{-1}$ ) is the mean wind speed.



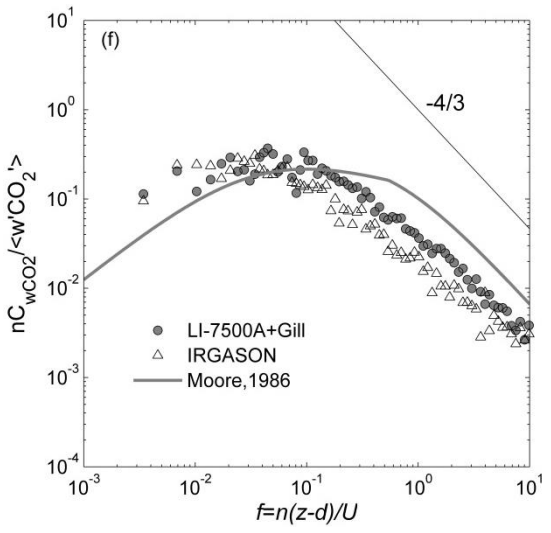
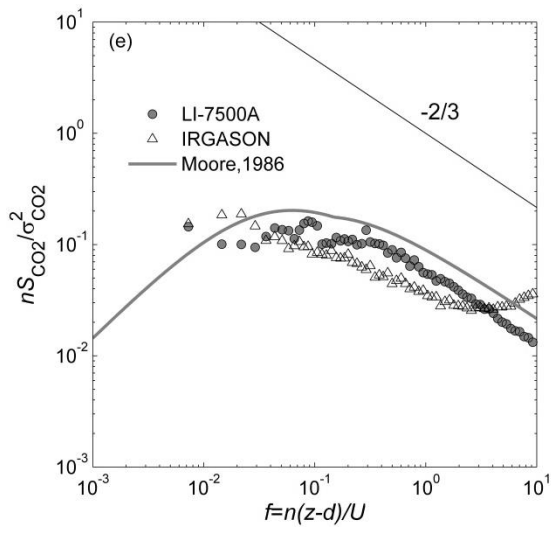


Figure S2 Relationship between sensible heat flux ( $H$ ) with the Gill and the IRGASON within favorable wind direction ( $0^\circ - 180^\circ$ ). Solid line represents geometric mean regression with regression statistics noted. The parameter range of the regression statistics represents 95% confidence bounds. The number of observations ( $N$ ), the index of agreement ( $I$ ) and the root mean square error (RMSE) are also indicated.

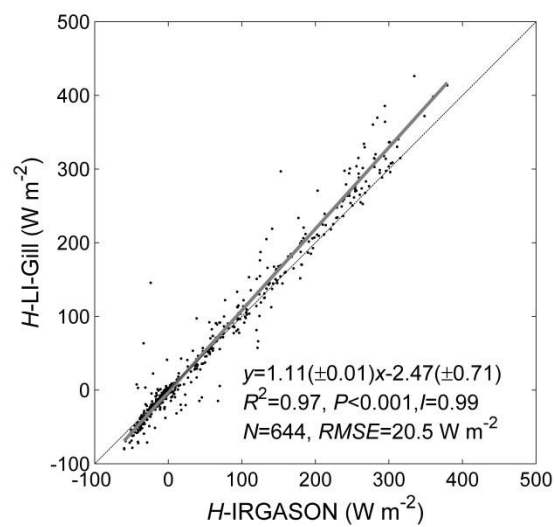


Figure S3. Time series of the CO<sub>2</sub> flux ( $F_c$ ) measured with the separated EC (LI-7500A + Gill) and air temperature ( $T_a$ ) during the winter experiment.

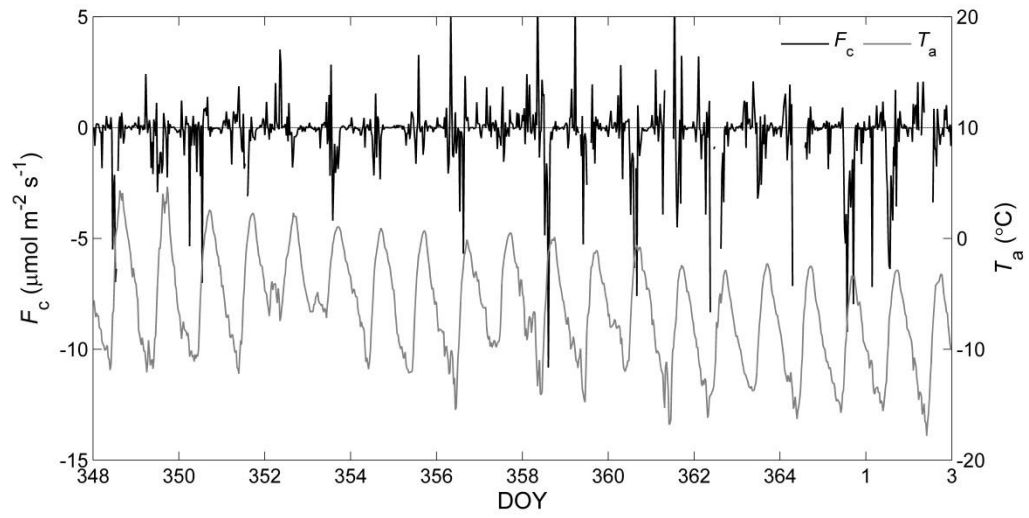


Figure S4. Scatter plot showing the WPL-corrected  $F_c$  comparison between the separated and the integrated EC system during the winter experiment for (a) full wind direction and (b) favorable wind direction ( $0^\circ - 180^\circ$ ). Solid line in represents geometric mean regression with regression statistics noted. The parameter range of the regression statistics represents 95% confidence bounds. The number of observations ( $N$ ), the index of agreement ( $I$ ) and the root mean square error (RMSE) are also indicated.

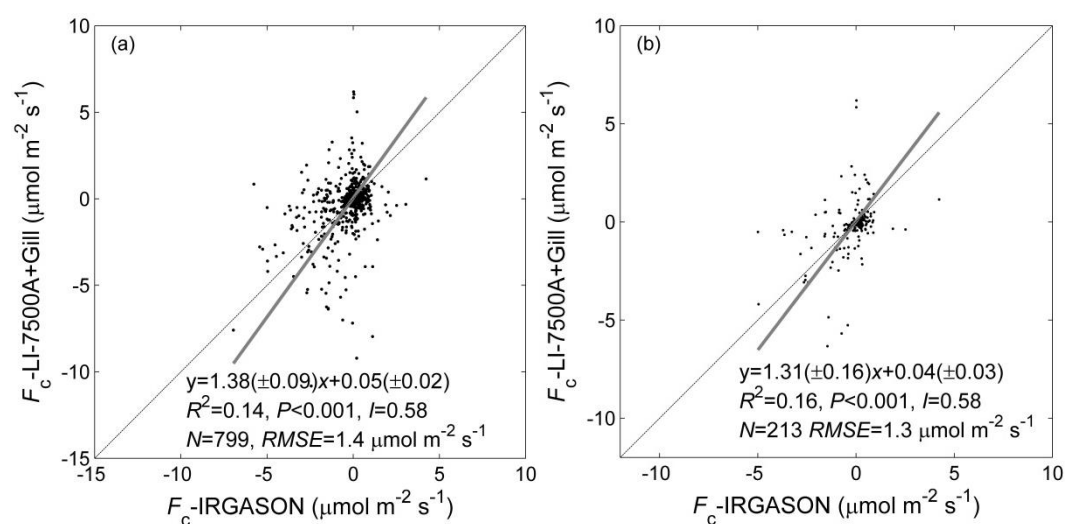


Figure S5. Diurnal composition of the density correction for separated EC  $F_c$  using (a) heat fluxes from separated EC (b) heat fluxes from IRGASON: the raw  $\text{CO}_2$  flux ( $F_{c\text{-raw}}$ ), temperature WPL correction ( $F_{c\text{-wpl-H}}$ ), water vapor WPL correction ( $F_{c\text{-wpl-H}_2\text{O}}$ , multiplied by 10),  $\text{CO}_2$  flux after the WPL density correction ( $F_c$ ).

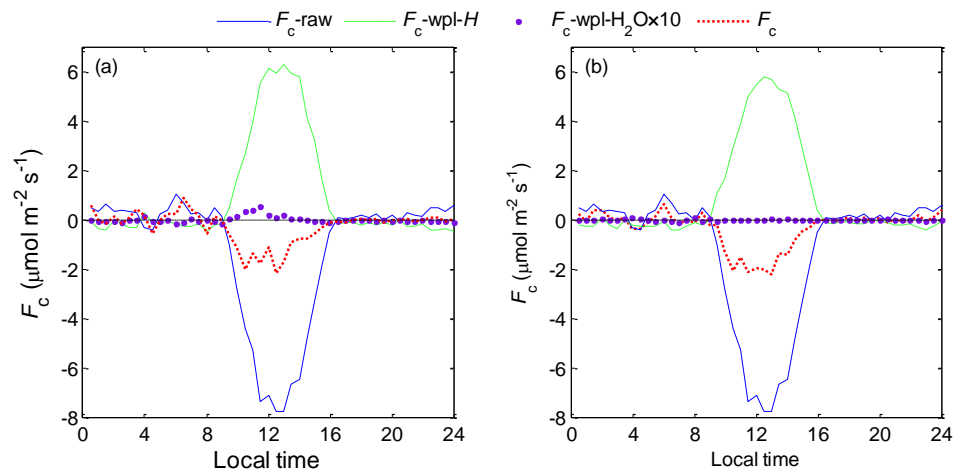


Figure S6. Relation between the latent heat flux ( $\lambda E$ ) with the separated and the integrated EC systems for (a) full wind direction and (b) favorable wind direction ( $0^\circ - 180^\circ$ ). Solid line represents geometric mean regression with regression statistics noted. The parameter range of the regression statistics represents 95% confidence bounds. The number of observations ( $N$ ), the index of agreement ( $I$ ) and the root mean square error (RMSE) are also indicated.

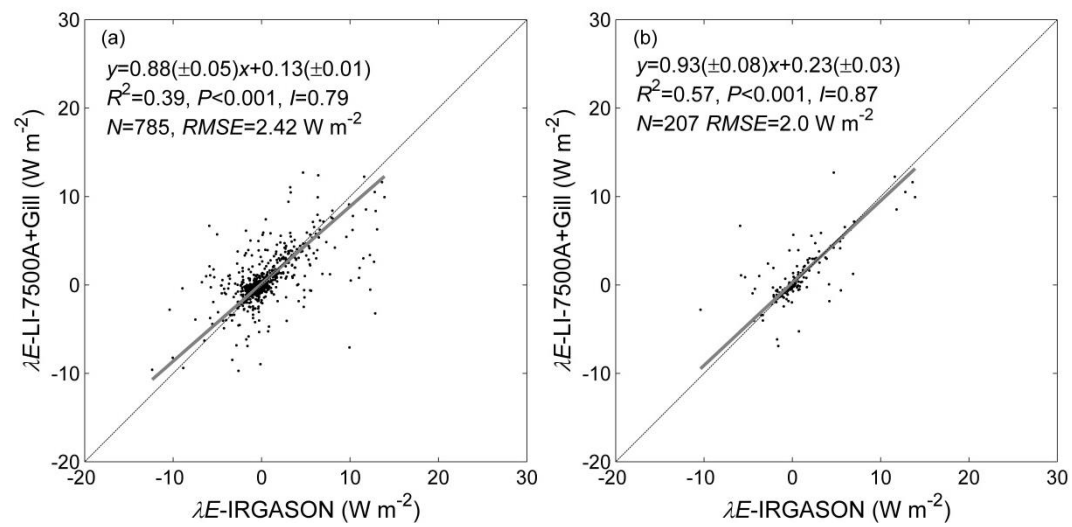


Figure S7. Relationship between the standard deviation of vertical wind speed ( $\sigma_w$ ) with the Gill and the IRGASON within favorable wind direction ( $0^\circ - 180^\circ$ ). Solid line represents geometric mean regression with regression statistics noted. The parameter range of the regression statistics represents 95% confidence bounds. The number of observations ( $N$ ), the index of agreement ( $I$ ) and the root mean square error (RMSE) are also indicated.

